Multidimensional Analysis of Nanoparticles with Highly Disperse Properties Using Multiwavelength Analytical Ultracentrifugation

Johannes Walter,[†] Konrad Löhr,[†] Engin Karabudak,[‡] Wieland Reis,[§] Jules Mikhael,[§] Wolfgang Peukert,[†,*] Wendel Wohlleben,[§,*] and Helmut Cölfen[⊥,*]

[†]Institute of Particle Technology (LFG), Friedrich-Alexander University Erlangen-Nürnberg (FAU), Cauerstr. 4, 91058 Erlangen, Germany, [‡]Faculty of Science & Technology, University of Twente, P.O. Box 217, 7500 AE Enschede, The Netherlands, [§]Material Physics Research, BASF SE, 67056 Ludwigshafen, Germany, and [⊥]Physical Chemistry, University of Konstanz, Universitätsstr. 10, 78457 Konstanz, Germany

ABSTRACT The worldwide trend in nanoparticle technology toward increasing complexity must be directly linked to more advanced characterization methods of size, shape and related properties, applicable to many different particle systems in science and technology. Available techniques for nanoparticle characterization are predominantly focused on size characterization. However, simultaneous size and shape characterization is still an unresolved major challenge. We demonstrate that analytical ultracentrifugation with a multiwavelength detector is a powerful technique to address multidimensional nanoparticle analysis. Using a high performance optical setup and data acquisition software, information on size, shape anisotropy and optical properties were accessible in one single experiment with unmatched accuracy and resolution. A dynamic rotor speed gradient allowed us to investigate broad distributions on a short time scale and differentiate between gold nanorod species including the precise evaluation of aggregate formation. We report how to distinguish between different species of single-wall carbon nanotubes in just one experiment using the wavelength-dependent sedimentation coefficient distribution without the necessity of time-consuming purification methods. Furthermore, CdTe nanoparticles of different size and optical properties were investigated in a single experiment providing important information on structure—property relations. Thus, multidimensional information on size, density, shape and optical properties of nanoparticulate systems becomes accessible by means of analytical ultracentrifugation equipped with multiwavelength detection.

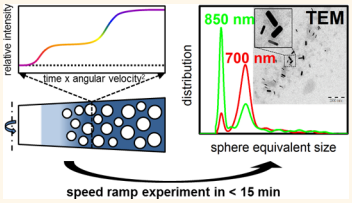

KEYWORDS: analytical ultracentrifugation (AUC) with multiwavelength detection · speed ramps · particle size distribution · nanoparticles · gold nanorods · carbon nanotubes

The accurate evaluation of particle size and shape distributions and optical information in particle technology is essential, both for scientific structure—property investigations and for commercial quality control. Their correct determination is indispensable more than ever because product properties are directly influenced by size and shape, and modern nanoparticle engineering would be impossible without the precise knowledge of the particle characteristics. Nanoparticulate systems have been shown to possess enhanced properties in a manifold manner. For very small semiconductor nanoparticles, quantum dots (QD), it was shown that the electro-optical properties[1] are a function of the particle size, making them a promising material in electronic devices and solar cells.[2] Although powerful methods were developed to get access to those systems within the last years,[3,4] their true multidimensional characterization is still not possible, and assumptions have to be made regarding the particle size-dependent optical properties. Shape anisotropic structures such as semiconductor or metallic rods and carbon nanotubes have various interesting properties, which can be used for thin film materials and optical applications.[5,6] However, the resulting product qualities are strongly dependent upon particle distribution and stability. Further examples include organic nanoparticles, like β-carotene, which have size- and structure-dependent optical properties.[7] Moreover, recent research has shown that the toxicology is strongly dependent on these disperse properties,[8−11]

* Address correspondence to wolfgang.peukert@fau.de, wendel.wohlleben@basf.com, helmut.coelfen@uni-konstanz.de.

Received for review December 19, 2013 and accepted August 17, 2014.

Published online August 17, 2014
10.1021/nn503205k

and the European regulatory definition of nanomaterials calls for precise size distributions.[12]

Many characterization techniques such as static and dynamic light scattering, field flow fractionation,[13] transmission electron microscopy, and chromatography among other techniques were developed for nanoparticle analysis. However, most of these methods suffer either from the complex inversion of ensemble measurements, the limited applicability for broad distributions or the underlying statistics. The latter is predominantly true for scanning or transmission electron microscopy and atomic force microscopy. Even though these methods provide highly accurate information on size, they are tedious and drying effects can impair the accuracy of particle counting, which is a clear drawback for the analysis of polydisperse samples. Usually, combinations of several time-consuming and expensive methods have to be employed for the evaluation of size, shape parameters, composition and optical characterization.

For almost 100 years, analytical ultracentrifugation (AUC) has been shown to be a very powerful and versatile tool for a number of important applications.[14] Because of very high rotor speeds up to 60 krpm, even particles with sizes in the lower nanoscale can be measured precisely and with Ångström resolution[15] with a variety of detectors such as single wavelength absorption, interference and fluorescence.[16] Even though biological systems were predominantly examined in the past, these detectors give access to almost every sample system in solution, *e.g.*, small metal or semimetal clusters,[17] polymers and biological macromolecules.[20,21] Even very small prenucleation clusters can be successfully separated from sedimenting salt ions.[18] Besides size analyses and information on shape anisotropy, samples can be examined with respect to their stability and interactions.[9,10] AUC was compared to other techniques in the above list and showed superior resolution for mixtures as well as the correct determination of particle concentrations.[19−21] Especially a study on latex mixtures performed worldwide in the laboratories of the Bayer group with various analytical techniques demonstrated the quality of AUC for particle size analysis in comparison to other techniques very well.[21]

The capabilities of AUC were further enhanced by the development of a multiwavelength UV−vis detector (MWL-AUC), which is capable of determining full UV−vis spectra for each detected species.[22,23] This detector was developed on an open source basis[24] and it was demonstrated that this detector can resolve complex mixtures and yield information about the sample components.[25,26] However, the first generations still had limited data quality, which at its best reached the quality of the commercial AUC, the Beckman-Coulter Optima XL-A/I.[23] For that reason as well as due to the limited reproducibility, this technique was never applied to complex mixtures to directly correlate hydrodynamic and spectral properties.

Although these developments significantly widened the possibilities of nanoparticle analysis, AUC is still a highly underrepresented and rarely applied technique for nanoparticle characterization. One of the major reasons could be the special challenges arising from these systems. Most of the particles in solution have a hybrid structure, in which a core particle is stabilized by attached ions or surfactants against agglomeration. As a result, the total particle density is often unknown and will change as a function of core size. This problem could be recently overcome by a simultaneous evaluation of sedimentation and diffusion coefficients, which yielded the density of monodisperse particles in a multicomponent mixture.[27] However, polydisperse particles still remain a challenge. The nature and binding of the surfactants is crucial for colloidal stability and hence many of the methods developed for biological systems cannot be directly transferred to particulate systems. This mainly affects the evaluation of heavy components and broad distributions, as it will be later discussed in our manuscript. Therefore, new methods are required addressing these and other particular challenges.

Herein, we describe a MWL-AUC with an improved optical setup and a new data acquisition software. We used preparative ultracentrifuges from Beckman Coulter (model Optima L-90K or Optima XL-80K) as a platform for our developments. These centrifuges allow a minimum rotor speed of 1 krpm and a maximum speed of 60 krpm in combination with the analytical 4-hole rotor. The spectrometer was positioned directly within the optical path, which leads to a substantially increased light sensitivity.[23] An UV−vis-enhanced optical fiber grants enhanced long-term stability due to reduced fiber bleaching. An UV-enhanced aluminum coated mirror replaced the prism, and the collimation was reworked in such way that a sheet shaped light profile is formed directly after the fiber. A new xenon flash lamp (Hamamatsu L-9455-1x) in combination with a high performance UV−vis CCD array spectrometer (Ocean Optics USB2000+ ES) allows to record full spectra every 3 milliseconds in a high-speed acquisition mode directly on the spectrometer memory. Recent mechanical drawings are provided *via* the openAUC framework. This setup guarantees a much more uniform intensity profile compared to the previous setups, thus providing a much better signal-to-noise ratio in the UV and NIR, as we will show later. We show that the improved data quality enabled us to perform high-end hydrodynamic analysis. Furthermore, continuous speed ramp experiments could be carried out, which are very useful for polydisperse particles using multiwavelength detection.[28] This new multiwavelength speed ramp functionality with a dynamic rotor speed gradient offers the

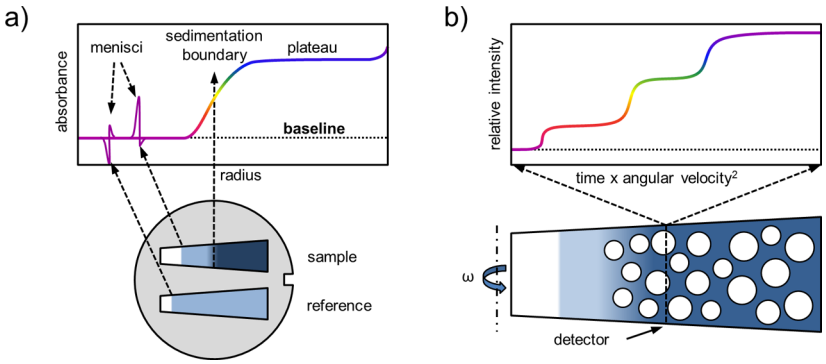

Figure 1. Measuring schemes of two different AUC experiments. (a) Sedimentation velocity experiment with scanning in radial dimension. (b) Speed ramp experiment at fixed radial position with variable rotor speed gradient.

possibility of measuring wide distributions on a very short time scale with high resolution. Using our high performance data acquisition software, the informational content of the measurements was improved significantly due to an enhanced sample capacity and detection capability. We validated all our developments with several polystyrene as well as protein standards and outline its potential for multidimensional particle analysis by means of gold nanorods, CdTe nanoparticles and single-/multi-wall carbon nanotubes. Plans of the setup can be obtained for free from the authors in the framework of the openAUC project (see also http://wiki.bcf2.uthscsa.edu/openAUC/). General schematic diagrams of the modified absorbance optics are also provided in the Supporting Information (SI).[24]

RESULTS AND DISCUSSION

Theoretical Foundations. In principle AUC is based on the optical detection of particle motion during their fractionation caused by a centrifugal field. For a sedimentation velocity experiment, this can be achieved with a detector measuring the flash light intensity as a function of time and space (Figure 1a). The apparent sedimentation coefficient is calculated as follows:

$$s = \frac{1}{\omega^2 t} \ln\left(\frac{r}{r_m}\right) \quad (1)$$

ω is the angular velocity, t the time, r the radial measuring and r_m the radial meniscus position. The sedimentation coefficient has the dimension of time and is usually expressed in Svedberg (1 S equals 10^{-13} seconds). Besides, we can use Stokes' law to transform the sedimentation coefficient to the equivalent diameter of a sphere with equal sedimentation and density:

$$d_{Stokes} = \sqrt{\frac{18\eta s}{\rho_p - \rho_s}} \quad (2)$$

d_{Stokes} is the diameter, η the solvent viscosity and ρ the solvent (s) and particle (p) density. The aforementioned equation only assumes sedimentation neglecting diffusion effects. The Lamm eq 3 gives a more accurate thermodynamic approach of the centrifugation process.[29,30]

$$\frac{\partial c}{\partial t} = \underbrace{D\left(\frac{\partial^2 c}{\partial r^2} + \frac{1}{r}\frac{\partial c}{\partial r}\right)}_{\text{diffusion}} - \underbrace{\omega^2 s\left(r\frac{\partial c}{\partial r} + 2c\right)}_{\text{sedimentation}} \quad (3)$$

$\partial c/\partial t$ is the change in mass concentration with time and D is the translational diffusion coefficient. Depending on the measurement conditions (*e.g.*, rotor speed, particle size, *etc.*), either the sedimentation or the diffusion is the dominant term. In particular, for particle sizes below 20 nm diffusion leads to a significant broadening of the particle size distribution (PSD), which has to be corrected. The translational diffusion coefficient of a small particle is defined by the Stokes–Einstein equation:

$$D = \frac{RT}{N_A f} = \frac{RT}{N_A 3\pi\eta d_H} \quad (4)$$

R is the gas constant, T the temperature in Kelvin, N_A the Avogadro's number, f the translational frictional coefficient and d_H the hydrodynamic diameter. Direct boundary modeling methods apply the mass conservation approach to the experimental data and evaluate sedimentation as well as diffusion. Eq 5 illustrates the hydrodynamic dependency of these values for a particle of arbitrary shape:

$$D(s, f/f_0) = RT[2(\rho_p - \rho_s)]^{1/2}[18s^{1/2}N_A\pi(f/f_0\eta)^{3/2}]^{-1} \quad (5)$$

f/f_0 is the frictional ratio, which is the friction factor divided by the friction factor of a sphere of equal volume. This ratio can be used to estimate shape parameters of particles in the case that the solvent and particle parameters are known. For various systems models were developed to characterize the dimensions and aspect ratios of rods, discs and plates based upon their friction.[31−34] Using the Kirkwood approximation and bead modeling it becomes even possible to calculate the friction coefficients for arbitrary shapes.[35,36] However, it has to be kept in mind that the frictional ratio represents in principle an infinite number

of different shapes that can have the same friction. Nevertheless, for systems of known geometry such as carbon nanotubes or nanorods, the frictional ratio can be used to estimate shape parameters.

The measurement and evaluation of very broad distributions poses considerable challenges for a classical AUC experiment since the sedimentation velocity scales with the square of the particle size. A multispeed analysis developed by W. Stafford is able to address this need because one sample is measured incrementally at multiple rotor speeds.[37] The sedimentation data from each speed are then combined into a single continuous distribution function. However, this is a very time-consuming procedure. Moreover, our experiments indicated that the stability of the sedimentation boundary is highly sensitive to the stepwise ramping for rotor speeds below 10 krpm. Furthermore, the evaluation of fast sedimenting species such as heavy particles is hardly possible in a sedimentation velocity experiment due to the limited temporal resolution (the particle sediments faster than the step motor is able to scan). For such systems it is the current state-of-the-art to change the solvent viscosity and/or density to slow down the sedimentation. This can either be achieved by ionic and nonionic additives or by using a more dense solvent such as ethylene glycol or glycerol. Although this is applicable to various macromolecules, for many particulate systems this is not an option. The stability of particles in solution is strongly dependent upon the interparticle forces. Specific ligands stabilize particles against agglomeration or particles are intrinsically stable due their surface chemistry. Thus, even a slight change of the solvent such as its polarity can lead to instable dispersions. For systems where primary particles as well as the degree of agglomeration are studied this is an inacceptable drawback. An exception are deuterated solvents because they normally do not affect the colloidal stability. However, for very dense particles the corresponding change in sedimentation velocity is negligible.

By keeping the measurement position constant no sedimenting species is missed and the examined distribution can be as broad as desired by varying the rotor speed gradient and the measurement duration (Figure 1b). In addition, lower rotor speeds extend the measuring range to particles of unit density (*e.g.*, polystyrene) up to 3 μm without changing the solvent conditions.[28] Disc centrifuges use this technique to measure PSDs, but they are limited to a single wavelength and their maximum speed is 24 krpm (10% maximum gravitational force of an AUC). Therefore, the smallest particle size is restricted to a few 10 nm. Moreover, disc centrifugation requires a standard sample of known size and density to be used for calibration. It cannot provide fundamental properties such as the sedimentation coefficient due to a lack of thermal control and the use of gradient liquids of unknown density/viscosity profiles. The latter is also problematic for systems that may specifically interact with the gradient liquids. The commercial analytical ultracentrifuges from Beckman Coulter achieve rotor speeds up to 60 krpm but do not give the possibility of speed ramps. A turbidity detector designed by the user community transferred this technique to the AUC and even though the particle size range could be extended by higher rotor speeds, the spectral dimension stayed inaccessible.[28,38,39] Herein, we implemented this indispensable function to our MWL-AUC giving numerous additional possibilities of sample analysis. It has to be noted that a 2-dimensional diffusion/shape analysis is not possible for a speed ramp experiment because the radial dimension is not recorded in such experiments.

For absorbance measurements, the measured attenuation can be expressed according to Lambert–Beer's law (within the linear range of concentration):

$$\ln\left(\frac{I_0}{I}\right) = \varepsilon c l \qquad (6)$$

I_0/I is the ratio of the light intensities of solvent and solution, ε is the extinction coefficient, c is the mass concentration and l is the path length. The extinction coefficient can be calculated based on Mie's scattering theory, which is applicable in a strict sense for spherical particles only.[40] It is dependent upon the extinction efficiency, the particle size as well as its density.[41] For absorbing particles, the absorbance as well as the scattering contributions have to be taken into account.[42] To obtain the correct concentrations for each species and distribution, the particle size and wavelength-dependent scattering has to be considered. The influence of Mie correction on size distribution was assessed in detail by M. D. Lechner.[42,43] For the time being, we only added scattering to the evaluation of the speed ramp data, since the only evaluation software available for speed ramp data by M. D. Lechner includes a scattering correction based on Mie theory by default.

Signal-to-Noise Performance. As an extension to the previous setup two or more flashes were averaged to keep the noise introduced by the flash-lamp and spectrometer as low as possible. A dark current correction was integrated to grant drift free operation. All absorbance data was calculated as follows: Either the radial intensity profile of a reference channel or the air above the sample's meniscus was used after the experiment to calculate an average intensity value for each run. This value was then used to calculate the absorbance. The last case led to pseudoabsorbance distributions. This procedure improved our signal-to-noise ratio (SNR) significantly because any intensity fluctuations of the reference were not taken into account. A wavelength averaging functionality was implemented to reduce the readout noise of the spectrometer and to provide an even better SNR.

In the data acquisition software a desired number of pixels can be specified for averaging. Herein, we averaged three pixels resulting in a theoretical spectral resolution of 1 nm. Since the absolute resolution defined by the diffraction grading is approximately 2 nm, up to 6 pixels can be averaged without losing any resolution. In Figure 2 the largely reduced intrinsic detector noise of our improved MWL-AUC is shown by comparing the results of a radial scan at 650 nm (an empty rotor hole) with the commercially available single wavelength absorption detection of the XL-A from Beckman Coulter.

Table 1 demonstrates the uniform detector noise of the MWL-AUC design in whole accessible spectrum, whereas the XL-A has a low SNR in the UV range only. The noise contribution is strongly dependent on the amount of light getting to the detector. The XL-A with its free beam arrangement is optimized to get a maximum signal in the UV range, which is mainly important for biological applications. For particulate systems, where the visible range is quite often important, this is a serious disadvantage due to the increased noise contribution there. For the MWL-design we observe a slightly higher standard deviation in the UV range due to the fiber coupling, but it performs better by a factor of 3 in the visible range compared to the XL-A. Therefore, our design is superior to the commercial AUC calling for manifold experimental studies including measurements in the UV, visible as well as NIR. Later on, this improvement will be highly beneficial for our studies on the multi-wall carbon nanotubes (mwCNTs).

Validation. The data acquisition (DAQ) software and the accuracy of the MWL-AUC were validated by means of Duke NIST traceable polystyrene (PS) standards and two standard proteins in sedimentation velocity experiments. To assess the quality of our MWL-AUC design several parameters can be applied such as the mass averaged diameter or the width of the distribution (*e.g.*, d_{90}/d_{10} or d_{75}/d_{25}). The weighting of the distribution (number, size, area, mass or intensity) is dependent upon the measurement technique. A different weighting will therefore lead to a different mean diameter. For absorbance based AUC data, the given values are mass weighted for small particles (<15 nm), which is a good approximation because the contribution of scattering is negligible. However, for bigger particles all distributions would have to be scattering corrected to give mass weighted distributions. The manufacturer of the PS latexes used photo correlation spectroscopy (PCS, intensity weighted) and TEM (number weighted) to determine the mean diameters including the expanded uncertainties of the measurement methods. For an accurate comparison, all distributions would have to be converted to match in weighting. Nevertheless, for our studies we used the integral average of the sedimentation coefficient to validate our design, since we did not apply scattering corrections. We think that this is a valid assumption to assess the quality of our device since the shift in the d_{50}-value is very small for the monodisperse systems, we considered for our validation experiments.[42] However, for polydisperse samples or mixtures of different latexes the mean value will significantly shift with weighting, which should in any case have to be taken into account.

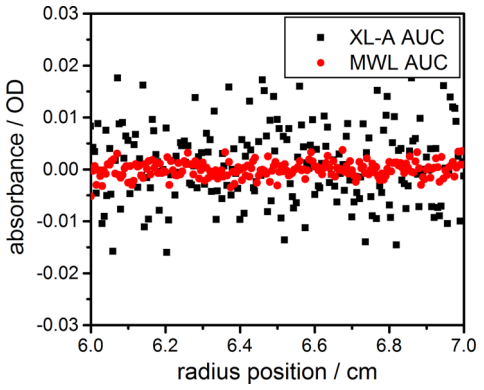

Figure 2. Comparison of the empty hole scans of MWL-AUC with those from a commercial XL-A measured at 650 nm with an equal number of radial data points and a scan duration of 2 min at 20 krpm.

TABLE 1. Wavelength-Dependent Absorbance of an Empty Hole Measurement of The MWL-AUC in Comparison to the Commercial XL-A with a Single Wavelength Absorbance Detector

	absorbance/OD	
wavelength/nm	XL-A	MWL
280	0 ± 0.00237	0 ± 0.00248
450	0 ± 0.00235	0 ± 0.00183
650	0 ± 0.00723	0 ± 0.00181

For polystyrene beads the mean sedimentation coefficients were converted to particle sizes using eq 2 using a specified density of 1.05 g/cm^3. Three different latexes with nominal particle sizes of 21 ± 1.5, 46 ± 2.0 and 498 ± 5 nm were measured. Sedimentation data, fits resulting from the data analysis, residuals and the obtained sedimentation coefficient distribution are exemplarily shown for the 46 nm size standard in Figure 3. For all standards the determined sizes are in a very good agreement to the PCS (21 nm) and TEM (46 and 498 nm) data provided by the manufacturer. The particle size measured for the smallest standard was 19.8 ± 0.3 nm (12.9 ± 0.4 S), which is smaller by 5.7%. We calculated the diameter of a sphere with equal sedimentation, which is influenced by any contributions of the stabilizer such as higher friction factor and decreased particle density. Prior studies have shown that surface ligands decrease the sedimentation rate due to an increased hydrodynamic diameter

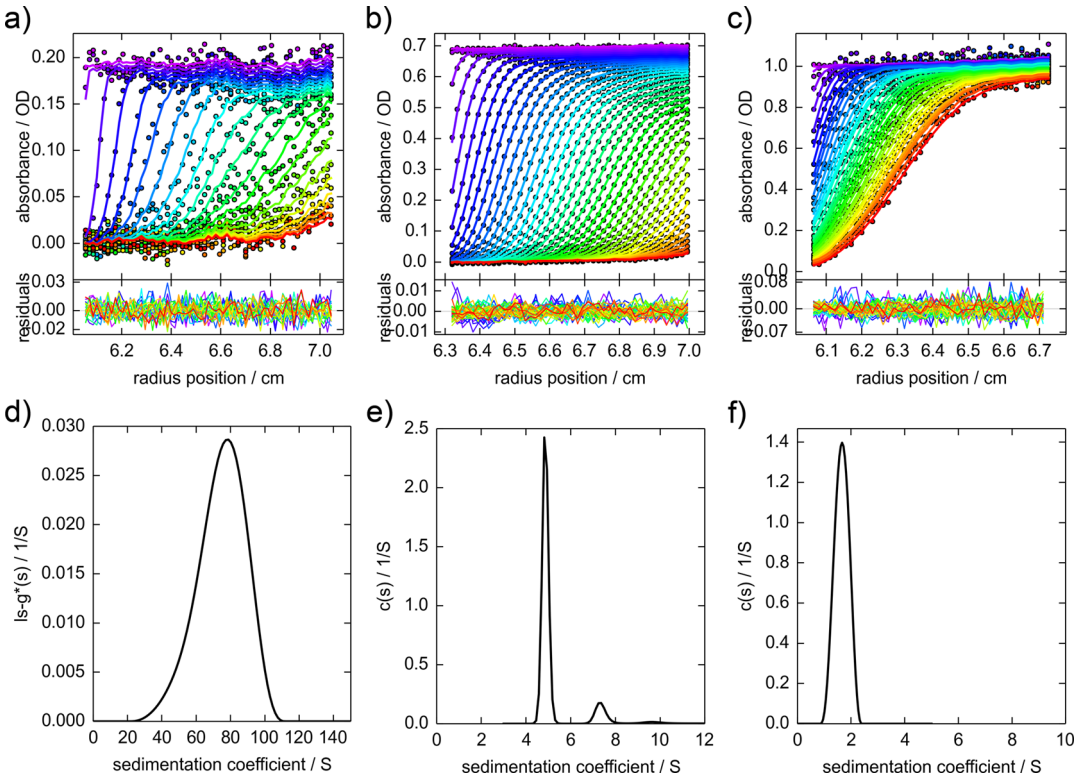

Figure 3. (a–c) Representative sedimentation velocity data and residuals of the validation experiments for 46 nm PS (λ = 300 nm), BSA (λ = 280 nm) and LSZ (λ = 280 nm). Symbols show every third data point of every third scan, and solid lines represent the best-fit boundary model obtained by the *c*(*s*) or ls-g*(s) analysis. Random noise level was dependent on the number of averages per position. RMSD values were always less than 0.02 OD, and runs test *Z* values (measure for the randomness of noise; see SI for more information) were always less than 10 for the validation experiments. (d–f) Best-fit normalized sedimentation coefficient distributions. All figures were created using GUSSI (http://biophysics.swmed.edu/MBR/software.html).

and a decreased particle density.[44] This difference gets higher as more stabilizer is added to the system and as the core size gets smaller. Hence, the particle size of 45.8 ± 1.9 nm (69.2 ± 5.8 S) for the medium beads almost matches the data of the manufacturer. The deviation of less than 0.5% is far below the value of 2%, which was shown as a typical value for AUC experiments with the commercial Beckman devices.[45] For the biggest polystyrene latex the evaluation required additional care. Even though we did not notice any rotor instabilities, particles sedimenting so quickly allow only a few scans to be used for data evaluation. Most importantly, the meniscus region gets blurred due to the low gravitational forces. Therefore, we fitted the meniscus position for this sample in Sedfit. For all other standards, the meniscus position was well-defined and did not change significantly when allowed to float during the fitting procedure. We determined a particle size of 482 ± 8 nm (7670 ± 239 S), which gives a deviation of 3.2% from the reference value. In our opinion this is a very good value for this type of centrifugation experiment. Because of the time-consuming calibration routines of the commercial AUC required before each experiment, such a system could hardly be measured using a commercial single wavelength absorbance detector. However, with our device this was not a problem as no further calibration was needed, so the experiment could start immediately. We reduced the typical minimum rotor speed of the commercial AUC from 3 krpm to 1 krpm for our system, thereby pushing the upper limit of detectable particle size by a factor of 9. In the aforementioned example, a rotor speed of 2 krpm was chosen allowing an optimum balance between sedimentation velocity and temporal resolution (the scanning time scales with the rotor speed). A total scan took 3 min for four samples with three averages each at every radial position. As mentioned previously, it would be desirable to slow down the sedimentation rate whenever possible to have a more accurate measurement. However, this will not work for many particulate dispersions because the colloidal stability may not be preserved. For such systems the MWL-AUC gives excellent results largely expanding the range of application. This could only be achieved by our enhanced measuring procedures, *e.g.*, fast and accurate radial and angular position calibration, ω^2t-calculation and the reduced noise contribution.

Thus far, we demonstrated the accuracy of our multiwavelength analytical ultracentrifugation design in a sedimentation velocity experiment. Moreover, we investigated a three component mixture of 97, 400 and

707 nm latexes using the speed ramp functionality. The experiment took 15 min with one data point every second and a continuous acceleration from 0 to 45 krpm at a radial detector position of 6.8 cm. The meniscus position was determined *via* a radial scan at the final rotor speed employed at the end of the experiment. In Figure 4 the evaluated data are represented. All three fractions can easily be identified with baseline resolution. The measured sizes and full width at half maximum (fwhm) were 87.5 nm (fwhm = 42.1 nm), 389.6 nm (fwhm = 118.1 nm) and 672.3 nm (fwhm = 154.6 nm), respectively. Thus, the absolute particle sizes are slightly shifted to smaller values (by 10, 3 and 5%, respectively). This is mainly induced by the inaccuracy of the meniscus determination, which was located at the end of the experiment at the highest rotor speed. The meniscus position gets shifted to higher radial positions with increasing rotor speed due to rotor stretching and solvent compression, causing the underestimation in the sedimentation coefficient, which is in fact most pronounced for the larger species. However, since the particle size scales with the square root of the sedimentation coefficient, higher absolute deviations will affect smaller sized particles more significantly, which explains the higher deviation for the smallest particle in the mixture.

A procedure addressing both, solvent compression and rotor stretching, would therefore be highly desirable. However, such a correction would be needed for each data point and the proprietary software used for the evaluations does not yet provide this option. The speed ramp method will never be as accurate as a sedimentation velocity experiment, since it discards boundary information due to the observation at one radial point only, but it is highly useful because very broad distributions can be studied on a short time scale. Even though some more adaptions have to be carried out in the future to reach equal quality in comparison to turbidity optics, the present data gives very promising results because it includes spectral information, which was not accessible beforehand. A more advanced application of this function on gold rods will be shown later on.

In the past analytical ultracentrifugation was extensively applied to characterize biological macromolecules.[14] Therefore, the accuracy of our design will be further confirmed by two of the most widely used and well-known standard proteins lysozyme (LSZ) and bovine serum albumin (BSA). For comparison with literature data, the sedimentation coefficient extrapolated to zero concentration for water at 20 °C $s_{20,w,0}$ is used for the protein studies, because this is the primary and system independent quantity. Moreover, the frictional ratios were fitted for these systems to derive the molecular mass of the proteins. The measured $s_{20,w,0}$ of LSZ, 1.8 S (literature 1.9 S[46]), and BSA, 4.32 ± 0.01 S

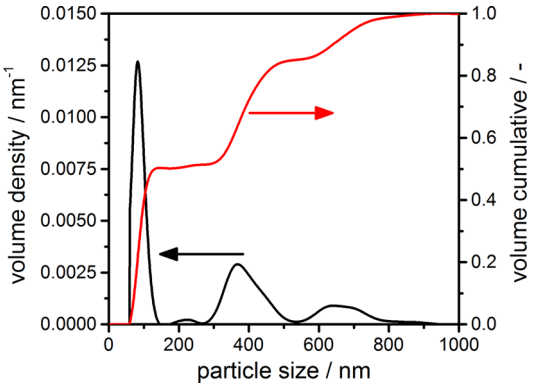

Figure 4. Mass weighted density and cumulative distribution of three component mixture of 100, 400 and 700 nm latexes measured in a speed ramp experiment (λ = 350 nm).

(literature 4.31 S[46]), are in a very good agreement with the expectations from literature. Sedimentation data, fits of the data analysis, residuals and the resulting sedimentation coefficient distributions (as measured, not normalized to standard conditions) are exemplarily shown for BSA and LSZ in Figure 3. For LSZ the frictional ratio was fitted to 1.27 (literature 1.22[47]−1.3[48]), which gave a molecular mass of 14.1 kDa (literature 14.3 kDa[49]). For BSA we fitted the frictional ratio to 1.34 (literature 1.3[50]), leading to a molecular mass of 65.8 kDa (literature 66.3 kDa[51]). Recent studies by Ghirlando *et al.* on the accuracy of the commercial AUC support our conclusion that the MWL-AUC gives more reliable results regarding the sedimentation coefficient.[52] They showed that the modern commercial XL-A/I AUCs gave an error as much as 10% for the sedimentation coefficient of BSA due to errors in the calibration routines, the temperature control and the w^2t calculations. They had to correct for all these parameters using numerous AUC devices and measurements to obtain a significantly reduced standard deviation of approximately 0.7%. With our device we matched the error corrected value of Ghirlando *et al.* immediately with 0.7% accuracy and without the need of any corrections. The values we obtained for the diffusion coefficients/frictional ratios are in the range we would expect for an AUC experiment.[14] Moreover, BSA was measured in quadruplicates (four different concentrations) on the other two MWL-AUCs (devices B and C) to validate the reproducibility through all systems. The sedimentation coefficients are 4.33 ± 0.01 S for device B and 4.30 ± 0.02 S for device C, which shows a very good reproducibility. Details of the obtained sedimentation profiles, sedimentation coefficient distributions, and fitting errors for the different devices are provided for the protein BSA in the SI.

Limit of Detection and Dynamic Range. The decreased noise contribution of the detector resulted in an enhanced detection capability, which is demonstrated by means of a concentration series of the PS 46 nm NIST traceable standard. PS was measured at concentrations

of 0.1, 0.5, and 2.0 g/L and gave reasonable diameter values of 45.0, 45.8 and 47.4 nm. The smallest concentration was examined in the spectral range from 250 to 700 nm to work out the limit of detection (LoD). The determined particle size was 47.8 at 700 nm with a ΔOD of 0.005 (RMSD = 0.002760; determined with and without noise fit). The total dynamic range (DNR) depends on the sample system and its extinction coefficient change in the recorded wavelength range. For the above-mentioned PS standard, a DNR of 1:300 (OD_{max} = 1.5) and a spectral DNR (ΔOD for 280 to 700 nm) of 1:50 was obtained. These considerations lead to the following expression for the DNR:

$$DNR_{measurement} = DNR_{OD} \cdot DNR_{spectral} = \frac{1}{300} \cdot \frac{1}{50} = 1{:}15000 \quad (7)$$

The DNR can be further increased to a value of 1:60 000 for this system using a 3 mm instead of a 12 mm centerpiece offering a highly flexible detection capability for numerous systems. The applied improvements of our setup led to an enhanced range of linearity, too. We do not want to examine this here in detail because this topic was already addressed in detail in a previous study.[23] For the CCD itself the linearity is better than 99% but it will be further affected by the contribution of stray light. This is in fact amplified by the anisotropic intensity profile of the applied xenon flash lamp. For measurements at low light levels, due to high absorbance or low light emission, this will negatively affect the linearity of the measurement. The aforementioned BSA measurements at 280 nm had a linearity of 99.4% (c_{max}/c_{min} = 4; $OD_{max} \approx 0.6$) and 94.7% (c_{max}/c_{min} = 8; $OD_{max} \approx 1.2$) determined by using the loading concentration measured by the AUC *versus* the dilution series. This is a very good result in comparison to recently reported data of the commercial XL-A with its monochromator based design.[52]

Besides, the LoD was studied by means of the reference material OECD-NM400, a mwCNT with an average diameter of 9 nm and a polydispersity in length (average 1.5 μm). This material has a very high extinction coefficient. Therefore, no significant influence of Schlieren effects or solvent-based nonideality was present due to the low concentrations investigated here (see Figure 5a for exemplary sedimentation data). Caused by the polydisperse distribution of diameters and lengths, the integrated sedimentation coefficient had uncertainties estimated at 529 ± 150 S depending on the concentration, which corresponded to an average particle size of the sphere equivalent diameter of 35 ± 5 nm. These deviations in the sedimentation coefficients can be explained due to the sample preparation as well as the data evaluation process. Very long tubes and aggregates easily got lost during the dilution series leading to a smaller mean particle size for the smallest concentration. For very high concentrations the limit of detector linearity was reached and very big fractions were lost or got underrepresented during the data evaluation routine, which leads to a smaller mean particle size. Even if the distributions were slightly shifted with concentration, the intrinsic polydispersity stayed the same, demonstrated by the almost constant $(s_{90} - {}_{10})/s_{50}$-value, which is 2.12, 2.30, and 2.37 from high to low concentration (see Figure 5b for the distribution). Detailed information about the underlying distributions can be found in Table 2. The characteristic sedimentation coefficient was retrieved down to a concentration of 0.005 g/L or 5 ppm. Previously, the ability of the commercial XL-I to quantify the content of mwCNTs in the presence of larger particles was determined for environmental samples down to only 50 ppm,[53] so the high SNR of the present setup further decreased the LoD by 1 order of magnitude. This result is of major importance for the classification of nanomaterials from a safety aspect, such as the release of CNTs from

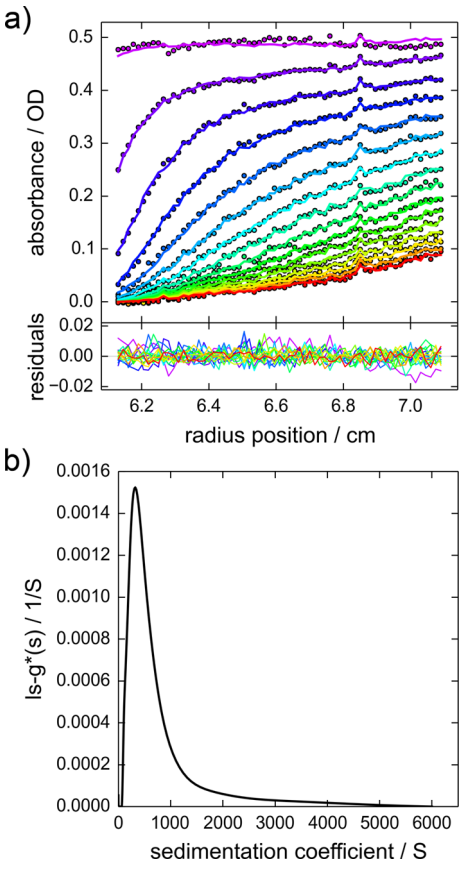

Figure 5. (a) Sedimentation velocity data and residuals of the OECD-NM400 experiment shown for the sample with a concentration of 0.2 g/L (λ = 700 nm). Symbols show every third data point of every third scan, and solid lines represent the best-fit boundary model obtained by the ls-g*(s) analysis. RMSD value was 0.0044 OD and runs test *Z* value was 18.23. (b) Best-fit normalized apparent sedimentation coefficient distribution.

TABLE 2. Sedimentation Coefficient Distribution Data As Well As Mean Particle Size of the Sedimentation Equivalent Sphere of Carbon Nanotubes (OECD-NM400)[a]

concentration/g/L	$s_{10}/s_{50}/s_{90}$/S	mean *s*/S	mean size/nm
0.2	161/406/1022	524.4	34.4
0.02	208/468/1284	676.0	39.1
0.005	72/198/541	387.5	29.6

[a] Data were evaluated at 700 nm (0.2 g/L), 500 nm (0.02 g/L) and 320 nm (0.005 g/L) to achieve the maximum SNR.

composite materials, since our MWL-AUC is not only able to determine particle size distributions but it also provides a superior LoD compared to the commercial centrifuges.

Mixture of Gold Nanorod Species. As a unique feature of the MWL-AUC, high-resolution size distributions and associated absorption spectra can be correlated. This is possible as an AUC experiment is sensitive to the sedimentation velocity and concentration of the particles. In an absorbance based AUC experiment, the absolute (*e.g.*, molar) concentrations of each species are constant but the measured extinctions will be a function of the wavelength. Depending on the systems examined, this dependency can be different for each species due to their unique optical characteristics. Using our MWL-AUC we are able to examine this wavelength dependency of the extinction coefficient for each species individually and directly in solution as long as the data evaluation gives stable peaks for all peaks and wavelengths. First, we demonstrate this by means of gold nanorods. Gold nanorods are very promising materials due to their plasmon-enhanced optical properties. A very comprehensive overview of the multiple properties of gold nanorods was recently presented by Chen *et al.*[54] Each gold nanorod has two characteristic optical responses, one corresponding to the longitudinal mode associated with the electron oscillations along the length axis and the other corresponding to the transverse mode excited by light polarized along the diameter of the rod.[55] Typically, the optical response measured for a mixture of nanorods is an integral over all species present in solution. Therefore, a tedious procedure is required for which monodisperse fractions have to be synthesized or purified to obtain the individual optical properties by UV–vis measurements. Herein, we show that it is possible to correlate hydrodynamic and optical properties using MWL-AUC, since the sedimentation rate will change with the hydrodynamic radius. Mixtures of two gold nanorods with different aspect ratios and longitudinal modes of approximately 700 nm (small aspect ratio species with large mass) and 850 nm (large aspect ratio species with small mass) were prepared. An absorbance spectrum of this mixture can be found in Figure S3 (SI). A transmission electron micrograph of the two different gold nanorods is shown in Figure 6a where the two different species can be clearly recognized. A speed ramp experiment of a mixture yielded the two gold nanorod species as shown in Figure 6b (solid lines). The differences in the population of the species (sedimentation equivalent diameters of 11.5 and 24.7 nm; a density 19.3 g/cm^3 was used for the calculation) are clearly wavelength-dependent, so the species must therefore have a different UV–vis spectrum (more wavelength-dependent PSD can be found in Figure S4 (SI)). Multiple analyses of the ramp data at different wavelengths would allow us to obtain the absorbance spectra for each species individually and directly in the mixture. Even though, no software exists up to now to evaluate such data, the manually performed evaluations already illustrate that the different spectral properties can be derived for each species using a speed ramp experiment. Furthermore, information about aggregation becomes accessible directly in solution with good resolution. To obtain the correct concentrations for each species and distribution, the particle size and wavelength-dependent scattering has to be taken into account. The only evaluation software available for speed ramp data by M. D. Lechner includes a scattering correction for spherical particles based on Mie theory, which cannot be applied to rod-like structures by definition. For the time being, we used this correction as a very first rough approximation. A comparison of the relative amount of the smaller species in the noncorrected raw data gave extinction weighted values of 10 and 45% at 700 and 850 nm, whereas the evaluated distribution gave relative amounts of 9 mass % and 48 mass %. Hence, the difference in concentration introduced by the scattering correction is small compared to the noncorrected data. No scattering correction was applied to other gold nanorod samples.

We performed a band sedimentation experiment on a mixture of the same gold nanorod species with different mixing ratio (the smaller species were less concentrated). This application shows the unique capability of our MWL-AUC to correlate the particle size distribution directly with the unique UV–vis spectra of all species present in the distribution in a single experiment. For such an experiment each radial position can be directly converted to a particle size employing eqs 1 and 2. The raw data of this experiment are shown in Figure 6c for a representative scan at 38 min. The graphs clearly show the fully resolved UV–vis spectra as a result of the sample fractionation in the radial domain (Figure 6d). For higher radial positions the absorbance at 700 nm becomes more pronounced, which is the characteristic peak corresponding to the species of smaller aspect ratio, which is sedimenting faster. As the corresponding video in the SI shows, the change of the UV–vis spectra according to the different sedimentation of the two gold nanorod species is clearly visible. Hence, the gradual changes of the

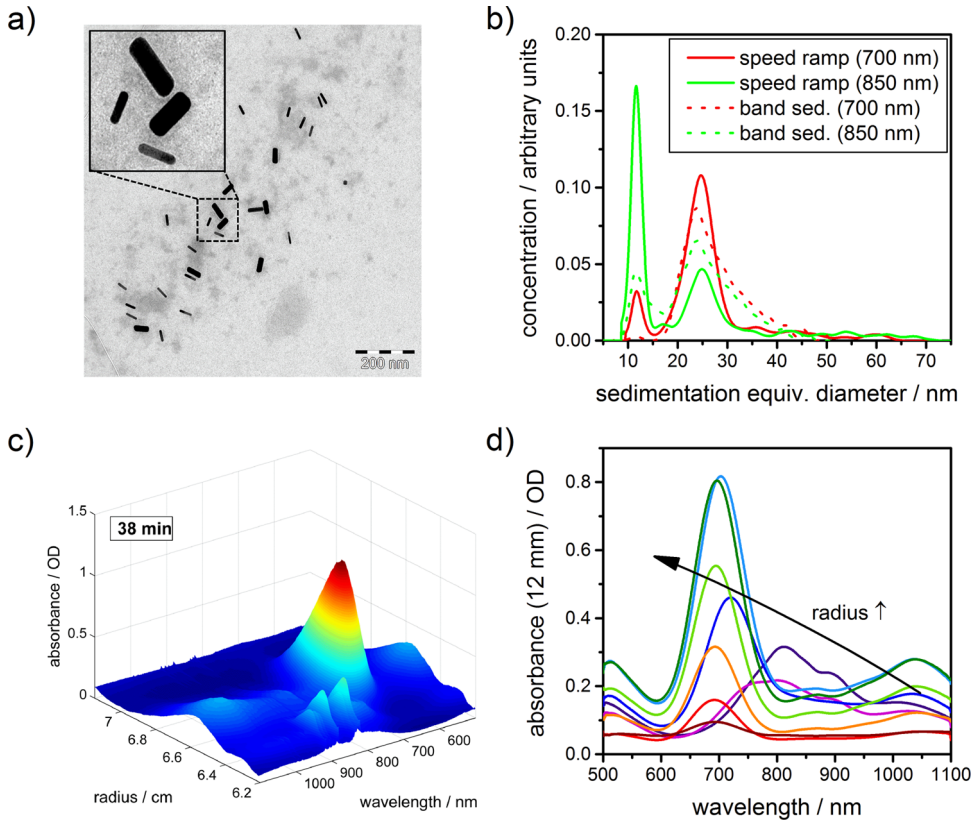

Figure 6. (a) TEM image of gold mixture clearly showing the two main species. (b) Extinction weighted particle size distribution of two mixtures of the same nanorod species gained at a speed ramp and band sedimentation experiment evaluated at 700 and 850 nm. (c) Multiwavelength spectra of gold-nanorods sedimenting at 2 krpm in a direct band centrifugation experiment as a function of the radial distance from the axis of rotation for a scan taken after 38 min. The 3D data surface is clearly visible. For a video, see SI. (d) Absorbance data of gold nanorods recorded in the radial dimension from 6.3 to 7.1 cm with 1 mm increment (purple to blue to green to red and arrow as a guide to the eyes) for the same snapshot (c) after 38 min in the band centrifugation experiment. A higher radial position results in an increased sedimentation equivalent diameter, which causes a blue-shift in the absorption spectrum due to the particle size and shape-dependent surface plasmon resonance.

UV−vis spectra with the distance from the center of rotation additionally demonstrate the fractionation of the gold nanorod binary mixture since already the raw data clearly show changes in the radially dependent spectra due to the fractionation of the two different particle sizes. In analogy to the speed ramp experiment, we evaluated the particle size distributions at the wavelengths of 700 and 850 nm using the analytical zone centrifugation ls-g*(s)-model in Sedfit (Figure 6b). Sedimentation equivalent particle sizes of 11.8 and 24.0 nm were obtained, which is very close to the values obtained from the speed ramp experiment (11.5 and 24.7 nm). Thus, the overlaid plots of the particle size distributions of speed ramp and band centrifugation experiment show the very good agreement between the two fundamentally different experiments. It should be noted that the absolute concentrations of each species cannot be trusted due to a lack of scattering corrections as well as the different loading concentrations for the two experiments.

In summary, the results in Figure 6 illustrate the advantage of the MWL detector over the previous approaches mainly based on particle size analysis by electron microscopy. AUC detects every species with high accuracy independent of the method used. As demonstrated by the results, the speed ramp experiment is especially suited for polydisperse samples, whereas the band centrifugation experiment allows direct correlation of spectral and hydrodynamic properties at a constant rotor speed. Since the scattering corrected absorption is directly proportional to the sample concentration, a further advantage is the quantitative concentration detection on the basis of all particles in solution rather than on those particles, which could be counted in TEM.

Single-Wall Carbon Nanotubes. Carbon nanotubes are carbon allotropes with a cylindrical shaped structure. The way graphene sheets are wrapped up is represented by the pair of numbers (*n*,*m*), also denoted by the chiral index, in which *n* and *m* designate the number of unit vectors along the cylindrical circumference of the honeycomb crystal lattice. Single-wall carbon nanotubes (swCNTs) have a wall thickness of just one graphene layer and are inherently a mixture of several (*n*,*m*) species after the production, with some species being semiconductors, some metallic.[56]

In order to derive structure–property relationships multistep purification protocols are required to isolate individual species, on which one can then perform spectroscopy.[57,58] These protocols require skills, know-how and many days of lab time. Here we show that it is possible to resolve individual (*n*,*m*) species within a well-dispersed, but only marginally purified mixture and that the unique absorption properties of the different species become accessible.

The SG65i batch contains tubes of various chiralities and was used previously by Fagan *et al.* in a highly purified form for the hydrodynamic analysis of the (*n*,*m*) = (6,5) species by means of AUC.[57] Figure 7a shows the absorbance spectra of the marginally purified sample used for our MWL-AUC study. Numerous absorbance peaks can be identified corresponding to transitions between the van-Hove singularities of the different tubes. The positions of these peaks are characteristic due to the different diameter of the tubes. The batch contains about 10 different chiralities, whereby detailed information can be obtained from the data sheet, which can be found online at the webpage of the manufacturer: http://www.swentnano.com/tech/docs/.

In our AUC analysis we considered three different wavelengths, whose peak maxima in the absorbance spectra correspond to three species. The absorbance maximum at 405 nm stems from a S33 transition, which has not been assigned to a specific chirality so far. However, it can be ruled out to be from the (6,5) or (8,3) nanotube.[59] The peak at 573 nm corresponds to the (6,5) chirality having a concentration of about 40% in the batch according to the data sheet of the manufacturer. This species was investigated in detail by Fagan *et al.*, too.[57] The peak at 670 nm corresponds most likely to the (8,3) chirality and is the most predominant one in this batch.[57] A simple data analysis was performed using the *c*(*s*) model in Sedfit at the different wavelengths with fixed values for the particle density (1.37 g/cm^3) and frictional ratio (4), which are typical for single-wall carbon nanotubes.[60] It was also checked that reasonable variations of such parameters do not change the basic shape of the distributions. As it can be seen in Figure 7b, several sharp peaks of sedimentation coefficients could be obtained. The sharp peaks can be explained due to self-sharpening, which is likely to occur during the sedimentation. This is a well-known phenomenon for elongated structures as well as some other nanoparticles, which narrows the widths of the peaks.[15,61−63] The peak positions are independent of the wavelength, but the peak integrals are clearly wavelength-dependent. Since the plotted data is represented as the non-normalized *c*(*s*)-distribution, each peak is directly proportional to the signal and thus to the extinction of a species sedimenting with a certain sedimentation velocity. This indicates that the peaks correspond to

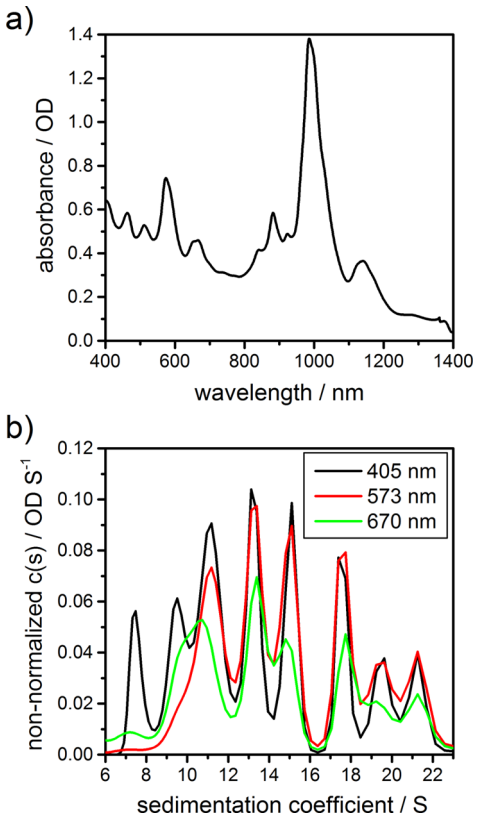

Figure 7. (a) Absorbance spectra of the SG65i swCNT batch from SouthWest NanoTechnologies, Inc. (b) Non-normalized sedimentation coefficient distributions evaluated at 405, 573 and 670 nm.

different species with different absorbance spectra. For example, the peak at about 11 S is likely to correspond to the (6,5) chirality, since this value was also measured on a highly purified, length- and diameter-sorted sample identified as (6,5) by its fluorescence.[57]

Further conclusions are not reasonable, since more detailed studies including 2-dimensional analysis would be required. However, for a 2-dimensional evaluation it has to be considered that the particle density is different for different chiralities due to the varying tube diameter. To investigate such dependencies, experiments in different H_2O/D_2O mixtures would be required to determine the anhydrous density for the surfactant-encapsulated swCNTs. The frictional ratio will then be a function of the tube length, and it was shown previously by Silvera Batista *et al.* that shape analysis is possible for carbon nanotubes of known density.[64] A detailed evaluation of those parameters of influence would exceed the focus of this paper and shall be discussed elsewhere. Instead, we wanted to propose a potential application taking advantage from the numerous capabilities made possible by the MWL-AUC. To extract the complete spectral information for each species, a simultaneous multiwavelength evaluation of the sedimentation velocity data with hundreds of wavelengths would be highly desirable as we have stated for the speed ramp experiments on gold,

too. Such evaluation cannot be performed with Sedfit because supercomputing with batch-processing would be required. Even though this is not possible at the moment, the software Ultrascan will soon be able to address this need.[65] This first evaluation clearly demonstrates the ability of MWL-AUC to distinguish differently colored species in a single experiment and to extract size-color correlations from mixtures of nearly identical materials that differ in diameter by fractions of a nanometer, thus eliminating the need to perform extensive purification before spectroscopy. In our opinion, multiple 2-dimensional spectrum analysis for different wavelengths including Monte Carlo analysis would be most suitable to address shape anisotropy and optical information simultaneously. Such developments are currently under progress for the software package Ultrascan.[47]

CdTe Nanoparticles of Different Size. Quantum confined semiconductor nanoparticles in the lower nanoscale, also referred to as quantum dots, are promising materials due to their size-dependent band gap $E(x)$. Thus, their optical properties are easily tuned by the particle size (distribution). For many materials, such as ZnO, PbS(e) and others, $E(x)$ is known very well.[66−69] However, for many materials (*e.g.*, copper indium selenide, doped or surface modified semiconductor materials) this information is not yet accessible due to the fact that those materials are comparatively new and not yet investigated in such detail like Cd- or Pb-based nanoparticles. Moreover, conventional analysis using a combination of TEM and UV−vis absorbance measurements is demanding and time-consuming. As shown beforehand, MWL-AUC is able to resolve size and optical properties individually in one experiment with a small sample volume. This makes it a highly promising technique for those materials. In the following, we will qualitatively demonstrate this capability of MWL-AUC to QDs by means of cadmium telluride (CdTe) nanoparticles. We investigated a mixture of three differently sized nanoparticle fractions obtained by size-selective precipitation. The normalized absorbance spectra of the individual fractions 1−3 derived by standard absorbance measurements are shown in Figure 8a. A clear red-shift of the absorbance maximum from 488 to 533 and 589 nm is observed with increasing particle size.

Figure 8b shows a 2-dimensional analysis of the sedimentation and diffusion coefficients, which was carried out at 488 nm due to the fact that all species are represented at this wavelength. The three different fractions can still be distinguished by means of their unique sedimentation and diffusion coefficients, even though the resolution of the Sedfit analysis is limited. According to the work of Carney *et al.* and Demeler *et al.* hydrodynamic diameters as well as particle densities can be derived using the data obtained by the 2-dimensional analysis on the sedimentation and diffusion.[27,70] Herein, we did no aim for such kind of quantitative analysis but want to emphasize instead the size-dependent optical properties of the CdTe QDs. Within one MWL-AUC experiment they are both directly accessible at the same time without the need of any complementary techniques. Already the raw data of the experiment, of which a snapshot is shown in Figure 8c, reveals the three differently

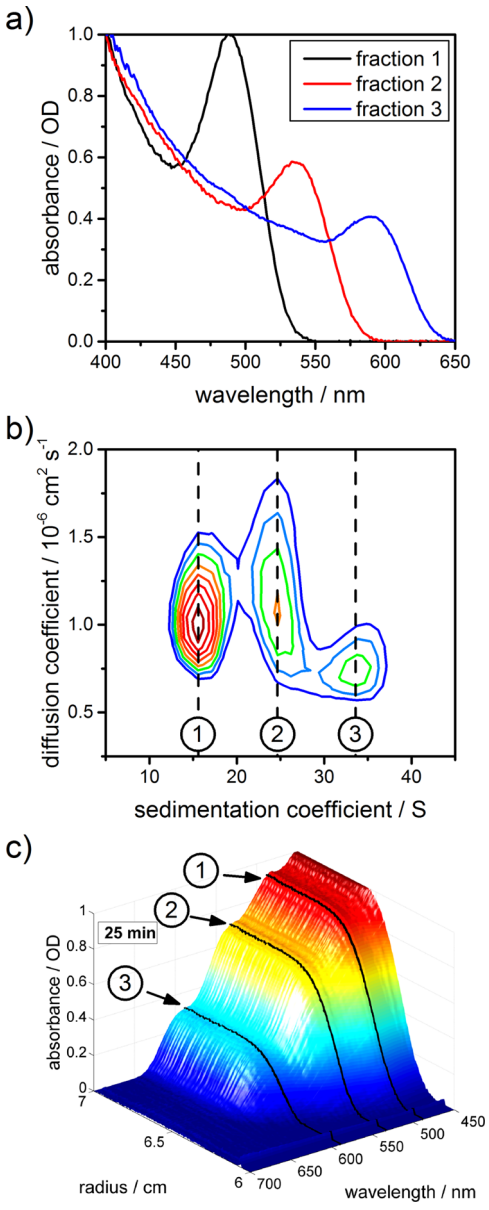

Figure 8. (a) Absorbance spectra of the three differently sized CdTe fractions used for the mixture. The maxima of the absorbance peaks are strongly red-shifted from fraction 1 to 3. (b) 2-dimensional analysis of sedimentation and diffusion at 488 nm using $c(s,f/f_0)$-analysis in Sedfit. The sedimentation coefficients of the three species are marked with dashed vertical lines as a guide to the eyes. (c) Multi-wavelength spectra of the CdTe mixture sedimenting at 30 krpm in a sedimentation velocity experiment as a function of the radial distance from the axis of rotation. The scan was taken after 66 min. The different peak wavelengths of the fractions are highlighted with black lines as a guide to the eye. The three species with their individual absorbance spectra and sedimentation rates are clearly distinguishable.

sedimenting species with their distinct absorbance spectra and specific peak maxima. A video of the complete sedimentation experiment can be found in the SI. By means of a 2-dimensional multiwavelength analysis of such MWL-AUC data, as proposed for the CNT experiments, unique information on QDs, *e.g.*, size-dependent properties, densities as well as hydrodynamic diameters, will become accessible. Especially the information on optical properties makes MWL-AUC clearly superior to single-wavelength AUC experiments. This will allow to study size-dependent properties of quantum dots throughout large parameter spaces (*e.g.*, not only size but also dopant concentration) with little experimental effort and with a small amount of material which is clearly not possible with conventional methodologies. This will in turn open new possibilities to get insights into the optical properties of QDs where a proper TEM analysis is not possible because of the remaining organics or where multiple samples with varying properties shall be examined (*e.g.*, hybrid structures with different amount of doping). In addition, we want to point out the much higher statistical relevance of AUC data as compared to TEM since every particle is detected.[19,21]

CONCLUSIONS

We showed that AUC equipped with a multiwavelength detector is a very powerful technique to address the multidimensional nanoparticle analysis. Optical and hydrodynamic properties can be examined simultaneously with very high accuracy and detection capability so far not accessible by any other technique. This provides access to various particulate systems, opening up new applications for this technique in science and technology, including characterization of proteins, particles with wide size distributions, plasmonic nanorods, carbon nanotubes and quantum dots as shown here. Strong methods are required facilitating the simultaneous hydrodynamic and optical characterization of MWL-AUC data. A novel speed ramp evaluation with enhanced functionalities, such as automatic MWL-evaluation, meniscus modeling and scattering correction is highly desirable. Coupling the sedimentation coefficient and absorption spectra would open the opportunity to directly obtain diffusion-corrected spectra for each component. This will be of high interest not only for carbon nanotubes or metallic rods but also for quantum dots, where it will be possible to evaluate the particle size-dependent optical information.

METHODS

Reference Materials. Nanosphere PS size standards were purchased from Fisher Scientific (3000 series; cat 3020A – Lot 33496, cat 3050A – Lot 32881, cat 3100A – Lot 32637, cat 3400A – Lot 23193, cat 3500A – Lot 32579, cat 3700A – Lot 33126) and were used as received. Concentration series were prepared *via* dilution with ultrapure water (18.2 MΩ cm^{-1}; total oxidizable carbon <10 ppb). For validation experiments using 21, 46 and 498 nm particles, four concentrations were measured three times each. BSA (A7030, purity ≥98%, essentially fatty acid free) and Lysozyme (L6876–10G, purity ≥90%) were purchased from Sigma-Aldrich and were used as received. Solutions were prepared by dissolving the protein in ultrapure water. Desired salt concentrations of 25 mM for the BSA solutions were adjusted by adding NaCl (purity ≥99.8%), Lysozyme was dissolved in 100 mM sodium acetate (purity ≥99%). Salts were purchased from Carl Roth.

Preparation of mwCNTs. 1 mg/mL of mwCNT (OECD NM400) from the OECD sponsorship program for nanomaterials were dispersed in H_2O and sonicated. The dispersion was then mixed with BSA resulting in the final dispersion of 1 mg/mL of nanomaterial and 5 mg/mL of protein as stabilizer.[71] The mwCNTs were measured in a dilution series from 0.2 to 0.005 g/L and were evaluated at wavelengths of 700, 500 and 320 nm.

Synthesis of Gold Nanorods. Gold nanorods were synthesized according to the methods of Ye and Nikoobakht.[6,72] Hexadecyltrimethylammonium bromide (≥99%), gold(III) chloride trihydrate (≥99.9%) and 2,6-dihydroxybenzoic acid (98%) were purchased from Sigma-Adrich. L-Ascorbic acid (98.7%) and sodium borohydride were purchased from Merck and silver nitrate (≥99.9%) was purchased from Carl Roth.

Synthesis of swCNT. Single-wall carbon nanotube powder was purchased from South-West Nanotechnologies (SG65 grade, lot# SG65i-L48). Sodium cholate hydrate (>99%) was acquired from Sigma-Aldrich and was used as received. swCNTs were dispersed *via* tip sonication (0.5 cm immersion depth, 1 h, Dr. Hielscher Up 200s, Tip: S2) in an ice bath at a nominal concentration of 0.1 mg/mL in a 2.0% aqueous sodium cholate hydrate solution. Following sonication, the resulting suspension was centrifuged in a high-speed centrifuge (Beckman Coulter Ultima XL-80k Ultracentrifuge, 250 000 *g*, 0.25 h), and the supernatant was collected. The last step was performed twice, iteratively.

Synthesis of CdTe Nanoparticles. Differently sized CdTe nanoparticles were synthesized using thioglycolic acid (TGA) as a stabilizer according to a procedure reported by Rogach *et al.*[73] All chemicals used were of analytical grade or of the highest purity available. All solutions were prepared using Millipore water as a solvent. The molar ratio of Cd^{2+}/Te^{2-}/TGA was 1/0.5/1.3, the pH of the synthetic mixture was adjusted to 12.[74] The nucleation and growth of the nanoparticles proceeded by refluxing at 100 °C under open-air conditions and was controlled by the reflux time. All samples were purified using size-selective precipitation by gradual precipitating nanoparticles induced by portion addition of an antisolvent (2-propanol) into a preliminary concentrated CdTe nanoparticle solution.[73]

AUC Measurements. Information about hardware has been previously presented in detail.[22,23] The system design software LabVIEW from National Instruments is used to handle the data acquisition. A light barrier measures the rotor speed and ensures the correct trigger cycle handles by a trigger box. Moreover, this signal is used to calculate the correct run time integral $\omega^2 t$-value, which is necessary for data evaluation. A xenon flash lamp from Hamamatsu (L-9455) and two different spectrometers from OceanOptics (USB 2000+ ES with different grating options) for the UV–vis and VIS-NIR were used. The rotor speed was 50/20/2 krpm for the polystyrene latexes (from small to large particle size, device A), 55 krpm for the proteins (device A and B/C for the BSA reproducibility studies), 10 krpm for the mwCNTs (device C), 40 krpm for the swCNTs (device C) and 25/30 krpm for the CdTe nanoparticles (device B). The band sedimentation experiment of the gold nanorods was carried out at 2 krpm (device B). The speed ramps reached from 0 krpm to 45 krpm for the latexes (device C) and from 3 krpm to

60 krpm for the gold nanorod mixture (device B). All sedimentation velocity data were acquired with a radial step of 50 μm. Titanium or aluminum centerpieces, path length 1.2 cm, were used for the sedimentation and speed ramp experiments. Epon based band forming centerpieces were used for the band sedimentation experiments. The time for temperature equilibrium was at least 1 h for all measurements.

AUC Data Evaluations. All sedimentation velocity data were evaluated using the Software Sedfit (Version 13.0b). The solvent and particle parameters for the validation experiments were calculated using the program SEDNTERP according to the method of Laue *et al.* (see Table S1 (SI) for detailed information).[75] All data were fitted to the *c*(*s*) continuous size distribution model, except the sedimentation data of the polystyrene beads and the gold rods, which were fitted to the ls-g*(s) size distribution model using Sedfit. All data were fitted with a second derivative regularization, a resolution of 100, time-independent and radial invariant noise and a regularization parameter of 0.95. The $c(s,f/f_0)$ was performed with a resolution of 40 in *s* and 20 in f/f_0 and regularization parameters of 0.683 and 0.95. All speed ramp data were evaluated with the technique developed by M. D. Lechner.

Characterization. UV−vis−NIR spectra were taken using a Varian Cary 50 spectrometer. For TEM imaging, one drop of the solution of gold nanorods was spread on a copper grid coated with a thin Formvar film and allowed to dry. Images were acquired with a Zeiss Libra instrument operating at an acceleration voltage of 120 kV.

Conflict of Interest: The authors declare no competing financial interest.

Acknowledgment. The authors would like to thank the German Research Council (DFG) for their financial support (Leibniz program) and the funding through the Cluster of Excellence Engineering of Advanced Materials and CRC 935 Carbon Allotropes. We also thank D. Haffke (University of Konstanz) for the skillfully performed experiments on the gold nanorods and Prof. Dr. Alexander Eychmüller, Dr. Nikolai Gaponik and Dr. Vladimir Lesnyak (all TU Dresden) for providing the CdTe nanoparticles. Cornelia Völkle is thanked for the AUC experiments on the CdTe nanoparticles.

Supporting Information Available: Schematic plans of the optimized setup, information regarding validation experiments, movie of band sedimentation experiment, absorption spectrum and PSD of gold nanorods, movie of CdTe sedimentation. This material is available free of charge *via* the Internet at http://pubs.acs.org.

REFERENCES AND NOTES

1. Spanhel, L. Colloidal ZnO Nanostructures and Functional Coatings: A Survey. *J. Sol-Gel Sci. Technol.* **2006**, *39*, 7–24.
2. Zhang, J.; Liu, H.; Wang, Z.; Ming, N. Shape-Selective Synthesis of Gold Nanoparticles with Controlled Sizes, Shapes, and Plasmon Resonances. *Adv. Funct. Mater.* **2007**, *17*, 3295–3303.
3. Pesika, N. S.; Stebe, K. J.; Searson, P. C. Relationship between Absorbance Spectra and Particle Size Distributions for Quantum-Sized Nanocrystals. *J. Phys. Chem. B* **2003**, *107*, 10412–10415.
4. Segets, D.; Gradl, J.; Klupp Taylor, R.; Vassilev, V.; Peukert, W. Analysis of Optical Absorbance Spectra for the Determination of ZnO Nanoparticle Size Distribution, Solubility and Surface Energy. *ACS Nano* **2009**, *3*, 1703–1710.
5. Voigt, M.; Klaumünzer, M.; Thiem, H.; Peukert, W. Detailed Analysis of the Growth Kinetics of ZnO Nanorods in Methanol. *J. Phys. Chem. C* **2010**, *114*, 6243–6249.
6. Ye, X.; Jin, L.; Caglayan, H.; Chen, J.; Xing, G.; Zheng, C.; Doan-Nguyen, V.; Kang, Y.; Engheta, N.; Kagan, C. R.; *et al.* Improved Size-Tunable Synthesis of Monodisperse Gold Nanorods through the Use of Aromatic Additives. *ACS Nano* **2012**, *6*, 2804–2817.
7. Auweter, H.; Haberkorn, H.; Heckmann, W.; Horn, D.; Luddecke, E.; Rieger, J.; Weiss, H. Supramolecular Structure of Precipitated Nanosize Beta-Carotene Particles. *Angew. Chem., Int. Ed* **1999**, *38*, 2188–2191.
8. Monopoli, M. P.; Aberg, C.; Salvati, A.; Dawson, K. A. Biomolecular Coronas Provide the Biological Identity of Nanosized Materials. *Nat. Nanotechnol.* **2012**, *7*, 779–786.
9. Schaefer, J.; Schulze, C.; Marxer, E. E. J.; Schaefer, U. F.; Wohlleben, W.; Bakowsky, U.; Lehr, C. M. Atomic Force Microscopy and Analytical Ultracentrifugation for Probing Nanomaterial Protein Interactions. *ACS Nano* **2012**, *6*, 4603–4614.
10. Walczyk, D.; Baldelli Bombelli, F.; Monopoli, M. P.; Lynch, I.; Dawson, K. A. What the Cell "Sees" in Bionanoscience. *J. Am. Chem. Soc.* **2010**, *132*, 5761–6758.
11. Zhu, M.; Nie, G.; Meng, H.; Xia, T.; Nel, A.; Zhao, Y. Physicochemical Properties Determine Nanomaterial Cellular Uptake, Transport, and Fate. *Acc. Chem. Res.* **2012**, *46*, 622–631.
12. Wohlleben, W. Validity Range of Centrifuges for the Regulation of Nanomaterials: From Classification to As-Tested Coronas. *J. Nanopart. Res.* **2012**, *14*, 1300.
13. von der Kammer, F.; Legros, S.; Larsen, E. H.; Loschner, K.; Hofmann, T. Separation and Characterization of Nanoparticles in Complex Food and Environmental Samples by Field-Flow Fractionation. *TrAC, Trends Anal. Chem.* **2011**, *30*, 425–436.
14. Scott, D. J.; Harding, S. S. E.; Rowe, A. J. *Analytical Ultracentrifugation: Techniques and Methods*; Royal Society of Chemistry: Cambridge, 2005.
15. Cölfen, H.; Pauck, T. Determination of Particle Size Distributions with Angström Resolution. *Colloid Polym. Sci.* **1997**, *275*, 175–180.
16. MacGregor, I. K.; Anderson, A. L.; Laue, T. M. Fluorescence Detection for the XLI Analytical Ultracentrifuge. *Biophys. Chem.* **2004**, *108*, 165–185.
17. Zook, J. M.; Rastogi, V.; MacCuspie, R. I.; Keene, A. M.; Fagan, J. Measuring Agglomerate Size Distribution and Dependence of Localized Surface Plasmon Resonance Absorbance on Gold Nanoparticle Agglomerate Size Using Analytical Ultracentrifugation. *ACS Nano* **2011**, *5*, 8070–8079.
18. Gebauer, D.; Völkel, A.; Cölfen, H. Stable Prenucleation Calcium Carbonate Clusters. *Science* **2008**, *322*, 1819–1822.
19. Dieckmann, Y.; Cölfen, H.; Hofmann, H.; Petri-Fink, A. Particle Size Distribution Measurements of Manganese-Doped ZnS Nanoparticles. *Anal. Chem.* **2009**, *81*, 3889–3895.
20. Cölfen, H.; Völkel, A.; Eda, S.; Kobold, U.; Kaufmann, J.; Puhlmann, A.; Göltner, C.; Wachernig, H. Mechanism of Nanoparticle-Enhanced Turbidimetric Assays Applying Nanoparticles of Different Size and Immunoreactivity. *Langmuir* **2002**, *18*, 7623–7628.
21. Lange, H. Comparative Test of Methods to Determine Particle Size and Particle Size Distribution in the Submicron Range. *Part. Part. Syst. Charact.* **1995**, *12*, 148–157.
22. Bhattacharyya, S.; Maciejewska, P.; Börger, L.; Stadler, M.; Gülsün, A.; Cicek, H.; Cölfen, H. Development of a Fast Fiber Based UV−Vis Multiwavelength Detector for an Ultracentrifuge. In *Analytical Ultracentrifugation VIII*; Wandrey, C., Cölfen, H., Eds.; Springer: Berlin, 2006; Vol. 131, pp 9−22.
23. Strauss, H. M.; Karabudak, E.; Bhattacharyya, S.; Kretzschmar, A.; Wohlleben, W.; Cölfen, H. Performance of a Fast Fiber Based UV/Vis Multiwavelength Detector for the Analytical Ultracentrifuge. *Colloid Polym. Sci.* **2008**, *286*, 121–128.
24. Cölfen, H.; Laue, T.; Wohlleben, W.; Schilling, K.; Karabudak, E.; Langhorst, B.; Brookes, E.; Dubbs, B.; Zollars, D.; Rocco, M.; *et al.* The Open AUC Project. *Eur. Biophys. J.* **2010**, *39*, 347–359.
25. Karabudak, E.; Wohlleben, W.; Colfen, H. Investigation of Beta-Carotene-Gelatin Composite Particles with a Multiwavelength UV/Vis Detector for the Analytical Ultracentrifuge. *Eur. Biophys. J.* **2010**, *39*, 397–403.
26. Karabudak, E.; Backes, C.; Hauke, F.; Schmidt, C. D.; Cölfen, H.; Hirsch, A.; Wohlleben, W. A Universal Ultracentrifuge Spectrometer Visualizes CNT−Intercalant−Surfactant Complexes. *ChemPhysChem* **2010**, *11*, 3224–3227.

27. Carney, R. P.; Kim, J. Y.; Qian, H.; Jin, R.; Mehenni, H.; Stellacci, F.; Bakr, O. M. Determination of Nanoparticle Size Distribution Together With Density or Molecular Weight by 2D Analytical Ultracentrifugation. *Nat. Commun.* **2011**, *2*, 335.
28. Mächtle, W. High-Resolution, Submicron Particle Size Distribution Analysis Using Gravitational-Sweep Sedimentation. *Biophys. J.* **1999**, *76*, 1080–1091.
29. Schuck, P. Size-Distribution Analysis of Macromolecules by Sedimentation Velocity Ultracentrifugation and Lamm Equation Modeling. *Biophys. J.* **2000**, *78*, 1606–1619.
30. Schuck, P. Diffusion-Deconvoluted Sedimentation Coefficient Distribution for the Analysis of Interacting and Non-Interacting Protein Mixtures. In *Analytical Ultracentrifugation: Techniques and Methods*; Scott, D. J., Harding, S. E., Rowe, A. J., Eds.; The Royal Society of Chemistry: Cambridge, 2005; pp 26−49.
31. Hansen, S. Translational Friction Coefficients for Cylinders of Arbitrary Axial Ratios Estimated by Monte Carlo Simulation. *J. Chem. Phys.* **2004**, *121*, 9111–9115.
32. Garcia de la Torre, J.; Huertas, M. L.; Carrasco, B. Calculation of Hydrodynamic Properties of Globular Proteins from Their Atomic-Level Structure. *Biophys. J.* **2000**, *78*, 719–730.
33. Garcia de la Torre, J.; Navarro, S.; Lopez Martinez, M. C.; Diaz, F. G.; Lopez Cascales, J. J. HYDRO: A Computer Program for the Prediction of Hydrodynamic Properties of Macromolecules. *Biophys. J.* **1994**, *67*, 530–531.
34. Tirado, M. M.; de la Torre, J. G. Translational Friction Coefficients of Rigid, Symmetric Top Macromolecules. Application to Circular Cylinders. *J. Chem. Phys.* **1979**, *71*, 2581–2587.
35. Garcia de la Torre, J. Building Hydrodynamic Bead-Shell Models for Rigid Bioparticles of Arbitrary Shape. *Biophys. Chem.* **2001**, *94*, 265–274.
36. Demeler, B.; Brookes, E.; Nagel-Stegert, L. Analysis of Heterogeneity in Molecular Weight and Shape by Analytical Ultracentrifugation Using Parallel Distributed Computing. *Methods Enzymol.* **2009**, *454*, 87–113.
37. Stafford, W. F.; Braswell, E. H. Sedimentation Velocity, Multi-Speed Method for Analyzing Polydisperse Solutions. *Biophys. Chem.* **2004**, *108*, 273–279.
38. Mächtle, W. Coupling Particle Size Distribution Technique. A New Ultracentrifuge Technique for Determination of the Particle Size Distribution of Extremely Broad Distributed Dispersions. *Angew. Makromol. Chem.* **1988**, *162*, 35–52.
39. Müller, H. G. Automated Determination of Particle-Size Distributions of Dispersions by Analytical Ultracentrifugation. *Colloid Polym. Sci.* **1989**, *267*, 1113–1116.
40. Mie, G. Beiträge zur Optik Trüber Medien, Speziell Kolloidaler Metallösungen. *Ann. Phys.* **1908**, *330*, 377–445.
41. Bohren, C. F.; Huffman, D. R. *Absorption and Scattering of Light by Small Particles*; Wiley-VCH Verlag GmbH: Weinheim, 2007.
42. Lechner, M. D.; Cölfen, H.; Mittal, V.; Völkel, A.; Wohlleben, W. Sedimentation Measurements with the Analytical Ultracentrifuge with Absorption Optics: Influence of Mie Scattering and Absorption of the Particles. *Colloid Polym. Sci.* **2011**, 1–11.
43. Lechner, M. D. On Mie Scattering. *J. Serb. Chem. Soc.* **2005**, *70*, 361–369.
44. Lees, E. E.; Gunzburg, M. J.; Nguyen, T.-L.; Howlett, G. J.; Rothacker, J.; Nice, E. C.; Clayton, A. H. A.; Mulvaney, P. Experimental Determination of Quantum Dot Size Distributions, Ligand Packing Densities, and Bioconjugation Using Analytical Ultracentrifugation. *Nano Lett.* **2008**, *8*, 2883–2890.
45. Cole, J. L.; Lary, J. W.; Moody, T. P.; Laue, T. M. Analytical Ultracentrifugation: Sedimentation Velocity and Sedimentation Equilibrium. *Methods Cell Biol.* **2008**, *84*, 143–179.
46. van Holde, K. E.; Johnson, W. C.; Ho, P. S. *Principles of Physical Biochemistry*, 2nd ed.; Pearson/Prentice Hall: Upper Saddle River, NJ, 2006.
47. Brookes, E.; Cao, W.; Demeler, B. A Two-Dimensional Spectrum Analysis for Sedimentation Velocity Experiments of Mixtures with Heterogeneity in Molecular Weight and Shape. *Eur. Biophys. J.* **2010**, *39*, 405–414.
48. Colvin, J. R. The Size and Shape of Lysozyme. *Can. J. Chem.* **1952**, *30*, 831–834.
49. Canfield, R. E. The Amino Acid Sequence of Egg White Lysozyme. *J. Biol. Chem.* **1963**, *238*, 2698–2707.
50. Fasman, G. D. *Handbook of Biochemistry and Molecular Biology: Proteins*, 3rd ed.; CRC Press: Cleveland, OH, 1976.
51. Hirayama, K.; Akashi, S.; Furuya, M.; Fukuhara, K. Rapid Confirmation and Revision of the Primary Structure of Bovine Serum Albumin by ESIMS and Frit-FAB LC/MS. *Biochem. Biophys. Res. Commun.* **1990**, *173*, 639–646.
52. Ghirlando, R.; Balbo, A.; Piszczek, G.; Brown, P. H.; Lewis, M. S.; Brautigam, C. A.; Schuck, P.; Zhao, H. Improving the Thermal, Radial, and Temporal Accuracy of the Analytical Ultracentrifuge through External References. *Anal. Biochem.* **2013**, *440*, 81–95.
53. Wohlleben, W.; Meier, M. W.; Vogel, S.; Landsiedel, R.; Cox, G.; Hirth, S.; Tomovic, Z. Elastic CNT-Polyurethane Nanocomposite: Synthesis, Performance and Assessment of Fragments Released During Use. *Nanoscale* **2013**, *5*, 369–380.
54. Chen, H.; Shao, L.; Li, Q.; Wang, J. Gold Nanorods and Their Plasmonic Properties. *Chem. Soc. Rev.* **2013**, *42*, 2679–2724.
55. Pérez-Juste, J.; Pastoriza-Santos, I.; Liz-Marzán, L. M.; Mulvaney, P. Gold Nanorods: Synthesis, Characterization and Applications. *Coord. Chem. Rev.* **2005**, *249*, 1870–1901.
56. Saito, R.; Hofmann, M.; Dresselhaus, G.; Jorio, A.; Dresselhaus, M. S. Raman Spectroscopy of Graphene and Carbon Nanotubes. *Adv. Phys.* **2011**, *60*, 413–550.
57. Fagan, J. A.; Zheng, M.; Rastogi, V.; Simpson, J. R.; Khripin, C. Y.; Silvera Batista, C. A.; Hight Walker, A. R. Analyzing Surfactant Structures on Length and Chirality Resolved (6,5) Single-Wall Carbon Nanotubes by Analytical Ultracentrifugation. *ACS Nano* **2013**, *7*, 3373–3387.
58. Hersam, M. C. Progress towards Monodisperse Single-Walled Carbon Nanotubes. *Nat. Nanotechnol.* **2008**, *3*, 387–394.
59. Liu, H.; Tanaka, T.; Urabe, Y.; Kataura, H. High-Efficiency Single-Chirality Separation of Carbon Nanotubes Using Temperature-Controlled Gel Chromatography. *Nano Lett.* **2013**, *13*, 1996–2003.
60. Backes, C.; Karabudak, E.; Schmidt, C. D.; Hauke, F.; Hirsch, A.; Wohlleben, W. Determination of the Surfactant Density on SWCNTs by Analytical Ultracentrifugation. *Chem.—Eur. J.* **2010**, *16*, 13176–13184.
61. Dhami, R.; Harding, S. E.; Jones, T.; Hughes, T.; Mitchell, J. R.; To, K.-m. Physico-Chemical Studies on a Commercial Food-Grade Xanthan—I. Characterisation by Sedimentation Velocity, Sedimentation Equilibrium and Viscometry. *Carbohydr. Polym.* **1995**, *27*, 93–99.
62. Mächtle, W.; Börger, L. *Analytical Ultracentrifugation of Polymers and Nanoparticles*; Springer-Verlag: Berlin, 2006.
63. Schachman, H. K. Physical Chemical Studies on Rabbit Papilloma Virus1. *J. Am. Chem. Soc.* **1951**, *73*, 4453–4455.
64. Silvera Batista, C. A.; Zheng, M.; Khripin, C. Y.; Tu, X.; Fagan, J. A. Rod Hydrodynamics and Length Distributions of Single-Wall Carbon Nanotubes Using Analytical Ultracentrifugation. *Langmuir* **2014**, *30*, 4895–4904.
65. Demeler, B.; Saber, H. Determination of Molecular Parameters by Fitting Sedimentation Data to Finite-Element Solutions of the Lamm Equation. *Biophys. J.* **1998**, *74*, 444–454.
66. Baskoutas, S.; Terzis, A. F. Size-Dependent Band Gap of Colloidal Quantum Dots. *J. Appl. Phys.* **2006**, *99*, 013708.
67. Segets, D.; Lucas, J. M.; Klupp Taylor, R. N.; Scheele, M.; Zheng, H.; Alivisatos, A. P.; Peukert, W. Determination of the Quantum Dot Band Gap Dependence on Particle Size from Optical Absorbance and Transmission Electron Microscopy Measurements. *ACS Nano* **2012**, *6*, 9021–9032.
68. Viswanatha, R.; Sapra, S.; Satpati, B.; Satyam, P. V.; Dev, B. N.; Sarma, D. D. Understanding the Quantum Size Effects in ZnO Nanocrystals. *J. Mater. Chem.* **2004**, *14*, 661–668.
69. Yu, W. W.; Qu, L.; Guo, W.; Peng, X. Experimental Determination of the Extinction Coefficient of CdTe, CdSe, and CdS Nanocrystals. *Chem. Mater.* **2003**, *15*, 2854–2860.

70. Demeler, B.; Nguyen, T.-L.; Gorbet, G. E.; Schirf, V.; Brookes, E. H.; Mulvaney, P.; El-Ballouli, A. a. O.; Pan, J.; Bakr, O. M.; Demeler, A. K.; *et al.* Characterization of Size, Anisotropy, and Density Heterogeneity of Nanoparticles by Sedimentation Velocity. *Anal. Chem.* **2014**, *86*, 7688–7695.
71. Nepal, D.; Geckeler, K. E. Proteins and Carbon Nanotubes: Close Encounter in Water. *Small* **2007**, *3*, 1259–1265.
72. Nikoobakht, B.; El-Sayed, M. A. Preparation and Growth Mechanism of Gold Nanorods (NRs) Using Seed-Mediated Growth Method. *Chem. Mater.* **2003**, *15*, 1957–1962.
73. Rogach, A. L.; Franzl, T.; Klar, T. A.; Feldmann, J.; Gaponik, N.; Lesnyak, V.; Shavel, A.; Eychmüller, A.; Rakovich, Y. P.; Donegan, J. F. Aqueous Synthesis of Thiol-Capped CdTe Nanocrystals: State-of-the-Art. *J. Phys. Chem. C* **2007**, *111*, 14628–14637.
74. Shavel, A.; Gaponik, N.; Eychmüller, A. Factors Governing the Quality of Aqueous CdTe Nanocrystals: Calculations and Experiment. *J. Phys. Chem. B* **2006**, *110*, 19280–19284.
75. Laue, T. M.; Shah, B. D.; Ridgeway, T. M.; Pelletier, S. L. Computer-Aided Interpretation of Analytical Sedimentation Data for Proteins. In *Analytical Ultracentrifugation in Biochemistry and Polymer Science*; Harding, S. E., Rowe, A. J., Eds.; Royal Society of Chemistry: Cambridge, 1992; pp 90−125.